Nanoscale Advances

ROYAL SOCIETY OF CHEMISTRY

PAPER

View Article Online
View Journal | View Issue

Cite this: *Nanoscale Adv.*, 2023, **5**, 742

Electrochemical analysis of glyphosate using porous biochar surface corrosive nZVI nanoparticles†

Aaliya Qureashi,[a] Altaf Hussain Pandith,*[a] Arshid Bashir,[a] Lateef Ahmad Malik,[a] Taniya Manzoor,[a] Faheem A. Sheikh,[b] Kaniz Fatima[a] and Zia-ul Haq[a]

Glyphosate [*N*-(phosphonomethyl)glycine] is a widely used phosphonate herbicide for different agricultural purposes. Due to its widespread use, suspected toxicity, and ubiquitous bioaccumulation, it is one of the most harmful contaminants found in drinking water. This demands efficient sensing and removal of glyphosate from contaminated water. Here, we report the decoration of novel and highly porous biochar with nanozero-valent iron (nZVI) nanoparticles to develop an efficient electrochemical sensor for the trace detection of glyphosate. The as-synthesized composite was thoroughly characterized by various state-of-the-art instrumental techniques. The electron micrographs of the composite materials revealed the cavity-like structure and the abundant loading of nZVI nanoparticles. FTIR and XPS analyses confirmed the presence of oxygen-rich functionalities and Fe(0) in the composite nanostructure. Electrochemical analysis through CV, LSV, and DPV techniques suggested efficient sensing activity with a limit of detection as low as 0.13 ppm. Furthermore, the chronopotentiometric response suggested excellent and superior stability for long-term applications. To gain more insight into the interaction between glyphosate and the composite material, DFT calculations were carried out. The Frontier Molecular Orbital study (FMO), Molecular Electrostatic Potentials (MEPs), and Density of States (DOS) suggest an increase in the electron density, an increase in the DOS, and a decrease in the HOMO–LUMO band gap by combining nZVI nanoparticles and biochar. The results suggest more facile electron transfer from the composite for trace detection of glyphosate. As a proof of concept, we have demonstrated that real-time analysis of milk, apple juice, and the as-synthesized composite shows promising results for glyphosate detection with an excellent recovery rate.

Received 8th September 2022
Accepted 13th December 2022

DOI: 10.1039/d2na00610c

rsc.li/nanoscale-advances

1. Introduction

Though organophosphorus pesticides (OPPs) such as glyphosate were extensively used for agricultural purposes, their suspected toxicity presents a significant challenge to the scientific community.[1,2] Glyphosates are one of the most widely used herbicides to control the growth of weeds, rodents, and long grass because they have been considered eco-friendly for an extended period. However, the consistent usage of glyphosate has resulted in the accumulation of its residues in water bodies, soil, and some foodstuffs. This cumulation of glyphosate has raised risk concerns over crop reliability, and ecological and environmental health.[3] Moreover, the primary degradation product of glyphosate, aminomethylphosphonic acid (AMPA), poses toxicity to humans and affects some vital organs.[4] Therefore, the design and the fabrication of magnetically recoverable composite materials with a promising prospect to detect and remove OPPs are highly desirable.

Several methods such as high-performance liquid chromatography,[5] capillary electrophoreses,[6] and gas chromatography[7,8] have been used to detect glyphosate. Despite their selectivity and high sensitivity, some shortcomings such as high cost and sample pre-treatment limit their use on a large scale.[9] Keeping this in mind, the development of electrochemical sensors has grabbed attention as they offer advantages in terms of a low cost, simple mode of operation, great sensitivity, specificity, and selectivity.[10] It is noteworthy to mention here that glyphosate is not electrochemically active; it becomes difficult to monitor glyphosate without modification of electrodes. In this regard, various materials such as MOFs,[11] chitosan,[12] layered double hydroxides,[13] gold nanoparticles,[14] zeolites,[15] CNTs,[16] and carbon-based electrodes[17] were reported in the literature for the electrochemical monitoring of glyphosate.

[a]*Laboratory of Nanoscience and Quantum Computations, Department of Chemistry, University of Kashmir, Hazratbal, Srinagar, J&K, India. E-mail: altafpandit23@gmail.com; Fax: +91-194-2414049; Tel: +91-194-2424900, +91-7006429021*

[b]*Department of Nanotechnology, University of Kashmir, Srinagar-190006, Kashmir, India*

† Electronic supplementary information (ESI) available. See DOI: https://doi.org/10.1039/d2na00610c

Biochar is a porous carbonaceous material obtained from the pyrolysis of different types of biomass. It has a strong prospect for its use in the abatement of environmental toxicants in wastewater management. The use of biochar offers several advantages such as a high surface area with a porous structure, less toxicity, abundant functional groups, and redox activity.[18] However, biochar-based materials have the limitations of less recovery and generation of secondary sludge. Therefore, there is emerging interest in the use of easily recoverable magnetically active materials owing to their superior properties such as magnetization, a large surface area with a strong affinity for contaminants, and easy recovery. So far, several magnetic materials have been continuously used for tuning the surface of biochar to enhance its surface charge capacity for better interaction and adsorption of organophosphorus pesticides.[19–21] In this arena of research, nano-zerovalent iron (nZVI) nanoparticles are the emerging magnetic material of choice due to their cost-effective nature, abundance, and active surface area with high reactivity. The nanoscale zero-valent iron (nZVI) is highly reactive toward the majority of pollutants such as dyes, antibiotics, heavy metal ions, and halogenated compounds.[22–27]

Under batch experimental conditions, nanoparticles are susceptible to aerial oxidation and agglomeration, which decreases the surface activity of the nanoparticles.[28] Among others, the impregnation of nZVI nanoparticles into porous material is ideal for the uptake of pollutants.

Herein, we report the synthesis of a nZVI@Biochar nanocomposite by adopting a simple ultra-sonication method. Various characterization techniques were employed to analyze and characterize the prepared magnetic biochar. The capacitive properties of nZVI and the prepared nanocomposites were inferred from magnetic studies. The as-synthesized magnetic biochar was found to be an efficient electrochemical sensor for glyphosate. The electrochemical response of the prepared sensor (nZVI@Biochar) for glyphosate was analyzed by utilizing cyclic voltammetry (CV), differential pulse voltammetry (DPV), and linear sweep voltammetry (LSV). The electrochemical sensing of glyphosate was further supported by DFT studies and the results were in complete harmony with each other.

2. Materials and methods

2.1. Materials

A lotus stem was collected from a local market, and iron(II) sulphate heptahydrate ($FeSO_4 \cdot 7H_2O$, > 99.0%), sodium borohydride ($NaBH_4$), glyphosate ($C_3H_8NO_5P$ > 98%), potassium nitrate (KNO_3 ≈ 98%), and KCl (>98%) were purchased from Sigma Aldrich. All the chemicals were of analytical grade and were used without further purification.

2.2. Synthesis of magnetic biochar (BC-nZVI)

The lotus stem, after being purchased from the local market, was washed and dried.[29] After drying the lotus stem was ground with a mortar and pestle for about an hour and then was carbonized in a muffle furnace for about 8 hours at a temperature of about 600 °C with a heating rate of about 10 °C min^{-1}. Finally, the black-colored material was dried overnight at 60 °C.

For the synthesis of the nZVI@Biochar nanocomposite, 1.6 g of biochar was dispersed in a three-necked flask containing 100 mL of 0.8 g L^{-1} $FeSO_4 \cdot 7H_2O$. For efficient adsorption of Fe^{2+} ions on biochar, the solution was continuously ultra-sonicated for eight hours. Thereafter, 50 mL of 0.2 M aqueous $NaBH_4$ was added dropwise into the flask to ensure the complete reduction of Fe^{2+} to Fe^0 under continuous N_2 gas purging. The

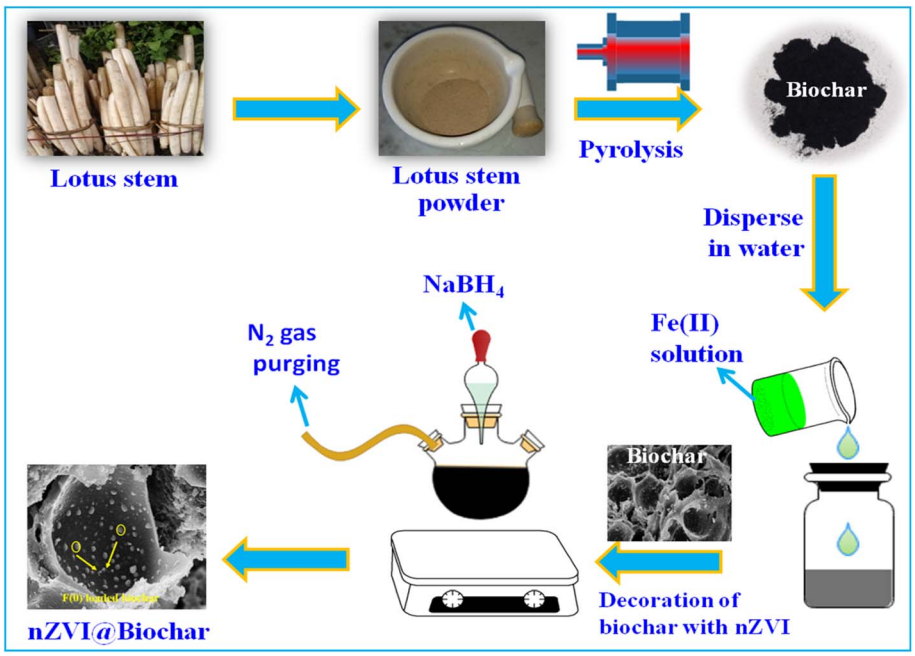

Scheme 1 Scheme representation for the synthesis of nZVI@Biochar.

reduction process involved in this step is according to Eqn (1). Moreover, the metal ions naturally present in the biochar such as Mg, Ca, Si, and P also undergo a reduction in the presence of sodium borohydride apart from zerovalent iron (nZVI). The as-synthesized magnetic biochar (nZVI@Biochar) nanocomposite was removed by applying an external magnetic retriever and was washed several times with ethanol and deionized water and finally was oven-dried at 30 °C (Scheme 1).

$$2Fe^{3+}\,(aq) + 6BH_4^-\,(aq) + 18H_20 \rightarrow 2Fe^0(s) + 6B(OH)_3\,(aq) + 21H_2\,(aq) \quad (1)$$

2.3. Characterization of magnetic biochar (BC-nZVI)

The structural integrity of BC, nZVI, and the nZVI@Biochar nanocomposite was characterized by Fourier transform infrared spectroscopy (FTIR) in the wavelength range of 4000–400 cm^{-1} using a PerkinElmer Spectrum-100 FTIR. The thermal stability of nZVI and nZVI@Biochar was analyzed by using a simultaneous thermal analyzer-STA (LINSEIS, USA 6807/8835/16) over a temperature range of 40 to 800 °C at a heating rate of 10 °C min^{-1}. The magnetic properties of BC, nZVI, and nZVI@Biochar were determined at room temperature using a vibrating sample magnetometer (Microsense E29). The surface morphology of BC, nZVI, and nZVI@Biochar was captured using a Zeiss Gemini SEM-500 Field Emission Scanning Electron Microscope (FE-SEM). The accelerating voltage was fixed at 10 KV and the images were captured at a magnification of 3, 15, and 100 K. The TEM micrographs of the as-synthesized materials were recorded by using a JEM-2010 analytical electron microscope, JEOL Ltd. The diffraction pattern of BC, nZVI, and nZVI@Biochar was recorded by using an X-ray diffractometer, Ultima-IV, Rigaku Corporation, Tokyo, Japan at 40 kV using a Cu Kα X-ray source ($\lambda = 1.5417$ Å). The X-ray photoelectron trace of nZVI@Biochar was obtained using a PHI 5000 Versa Probe III XPS instrument having monochromatized Al Kα ($E = 1486.7$ eV).

2.3.1. Analysis of natural samples. To investigate the practical efficacy of the nanocomposite material, a spike/recovery method was used to detect trace amounts of glyphosate in apple juice and milk. Fresh apple juice and industrially refined milk were spiked with different concentrations of glyphosate. Linear sweep voltammetry measurements were carried out to check the presence of glyphosate in these samples.

2.4. Electrochemical studies

The electrochemical studies, such as linear sweep voltammetry (LSV), cyclic voltammetry (CV), and differential pulse voltammetry (DPV), were carried out with a Biologic Potentiostat (VMP-300). All the measurements were carried out in a 3-electrode setup. The working electrode was prepared by drop-casting a known amount of biochar, nZVI, and nZVI@Biochar dispersed in isopropyl alcohol (IPA) on a glassy carbon electrode with Ag/AgCl as a reference and platinum mesh as the counter electrode. All the experimental conditions concerning detection were thoroughly optimized before taking the final results. For electrochemical sensing, two important things that need to be optimized are the potential window and pH conditions. We first optimized the potential window and then pH conditions. Since the reduction peak was found around −0.3 V at all pH, LSV and DPV were performed in this range only. Both LSV and DPV were performed starting from as low as possible concentration of glyphosate which increased slowly till a linear range was observed in both cases. For sensing parameters, studies were carried out by taking different concentrations of glyphosate in 0.1 M KNO_3 solution. CV and DPV studies were carried out by sweeping the potential between −1 V and +1 V at a scan rate of 10 mV s^{-1}.

2.5. Computational studies

The electrochemical sensing and the interaction of glyphosate can further be dealt with DFT calculation studies. All the DFT studies were carried out by using the Gaussian 03 set of codes. The geometries were optimized by using a Becke's three-parameter model system using the Lee–Yang–Parr correlation functional (B3LYP) and LanL2DZ basis set for the Fe atom and 6–311 g (d,p) for non-metal atoms.

3. Results and discussion

3.1. Characterization of the material

The synthesis of the nZVI@Biochar nanocomposite was carried out by a facile and wet impregnation method. To validate the formation of biochar and the incorporation of nZVI within the graphitic framework, we recorded the FTIR spectra of the samples. The FTIR spectra of nZVI, biochar, and nZVI@Biochar samples are shown in Fig. 1a. nZVI, biochar, and nZVI@Biochar present a characteristic vibrational band in the range of 3000–500 cm^{-1} that corresponds to the stretching vibration of –OH groups. The bands in the region of 1380–1430 cm^{-1} indicate the C–H bending of the methyl groups. The bands around 1600 cm^{-1} arise due to the bending vibration of the H–O–H bond along with the presence of C=C aromatic stretching vibrations. The broadband at 1026 cm^{-1} suggests C–O bending vibrations in the ester group. The weak vibrational band at 540 cm^{-1} indicates the presence of an Fe–O bond in nZVI. The weak vibrational band at 595 cm^{-1} in the composite confirms the successful impregnation of iron oxide on the surface of biochar. All these results suggest the successful formation of biochar and the nZVI @Biochar composite.

The XRD spectra of biochar show a diffraction peak at $2\theta = 27°$ which is indicative of the amorphous nature of biochar. The sharp diffraction peak at $2\theta = 45°$ assigned to the 110 plane in the nZVI@Biochar nanocomposite is due to the presence of face-centered α-Fe^0 particles, which indicates successful coating of nZVI on biochar (see Fig. 1b). Moreover, the other less intense peaks present in the XRD spectrum are probably due to iron oxide impurities on the surface of biochar, as reported in the literature.[30] The thermograms of the as-synthesized materials nZVI and nZVI@Biochar are shown in Fig. 1c, where it is evident

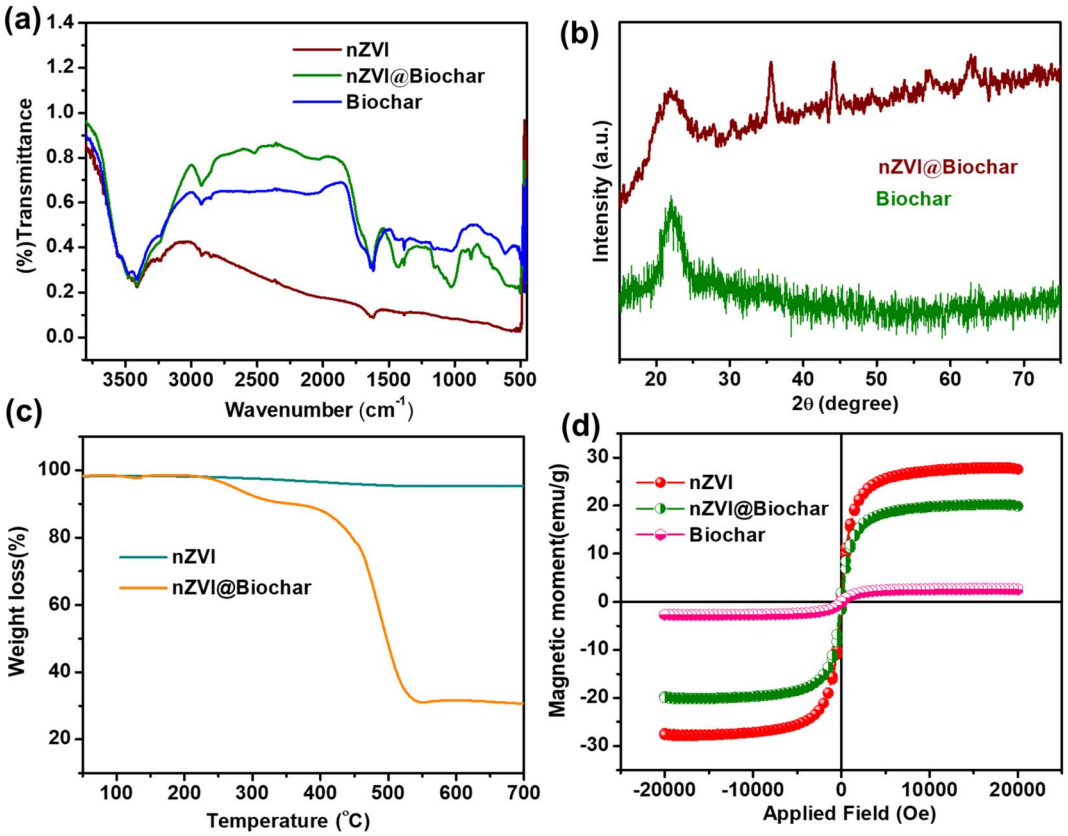

Fig. 1 (a) FT-IR spectra of biochar, nZVI, and the nZVI@Biochar composite, (b) XRD comparison between nZVI@Biochar and biochar, (c) TGA showing the mass change in the nZVI@Biochar composite as compared to nZVI, and (d) magnetic studies of biochar, nZVI, and the nZVI@Biochar composite.

that in the case of nZVI there is a small weight loss which is due to the adsorbed moisture over the surface of nZVI. Compared with the nZVI@Biochar nanocomposite thermogram, it exhibits a two-stage weight-loss behavior. At first, there was not any significant weight loss up to 240 °C. After 240 °C and up to 300 °C, there was a slight drop in the weight of around 7%, which is attributed to the decomposition of volatile matter. Subsequently, a second weight loss of about 50% was observed from 390 °C to 560 °C due to the thermal degradation of hemicellulosic and cellulosic content present in the biochar. Above 560 °C, no further weight loss was observed which indicates the complete carbonization and decomposition of the different units of biochar present in the nZVI@Biochar nanocomposite. Therefore, it can be concluded that the composite (nZVI@-Biochar) contains up to 30% nZVI, which proves the successful modification of biochar.

The magnetic properties of the as-prepared materials were determined by Vibrating Sample Magnetometry at room temperature (see Fig. 1d). As can be seen from the figure, the saturation magnetization of nZVI was around 27.93 emu g^{-1} and for the prepared nanocomposite (nZVI@Biochar) it was 17 emu g^{-1}. The rationale for the decrease in the saturation magnetization value of nZVI@Biochar was due to the presence of a non-magnetic biochar component. Other such similar reports are available in the literature.[30]

The structural integrity of the nanocomposite material was investigated using XPS analysis (Fig. 2a). The main composition of the prepared nanocomposite is C, O, and Fe with a small amount of sulfur. The C 1s spectra of nZVI@Biochar can be deconvoluted into three peaks at 284.7, 286.90, and 287.2 eV, which can be attributed to the presence of C–C and C–O bonds, respectively (Fig. 2b). Likewise, the O 1s spectra show two peaks around 530.48 and 528.26 eV, which indicate the presence of various oxygen-containing functional groups (C–O, C–OOH, and C=O) respectively, and the 527.99 eV peak is due to the presence of an Fe–O bond (Fig. 2c). For iron Fe 2p spectra, the specific binding energy peaks at 712, 709, and 707 eV were ascribed to the presence of Fe^{3+}, Fe^{2+} and Fe^{0}, respectively (Fig. 2d). The data are in agreement with those reported in the literature.[31]

Lotus, which is botanically called *Nelumbonucifera*, possesses an underwater stem that maintains air pockets throughout the length. The lateral cross-section, as shown in Fig. 3a and b, shows a wheel-like structure with pores in a symmetrical fashion, and the horizontal cross-section (see Fig. 3c and d) shows that the pores extend throughout the length of the stem, which is justified by FE-SEM micrographs. This porous nature of the lotus stem can be exploited as a raw material for designing high surface area and porous materials for a wide range of applications. In our case, we used it as a raw material

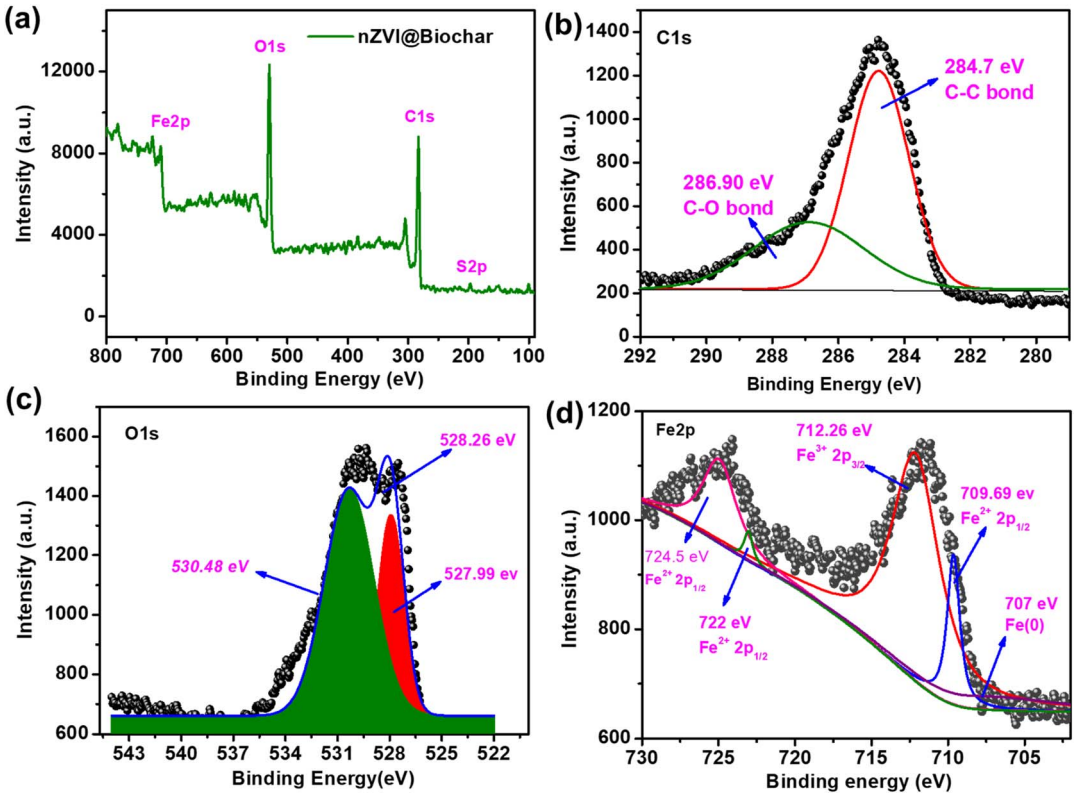

Fig. 2 (a) Compete range XPS, (b) C 1s XPS, (c) O 1s XPS and (d) Fe 2p spectra of the nZVI@Biochar composite.

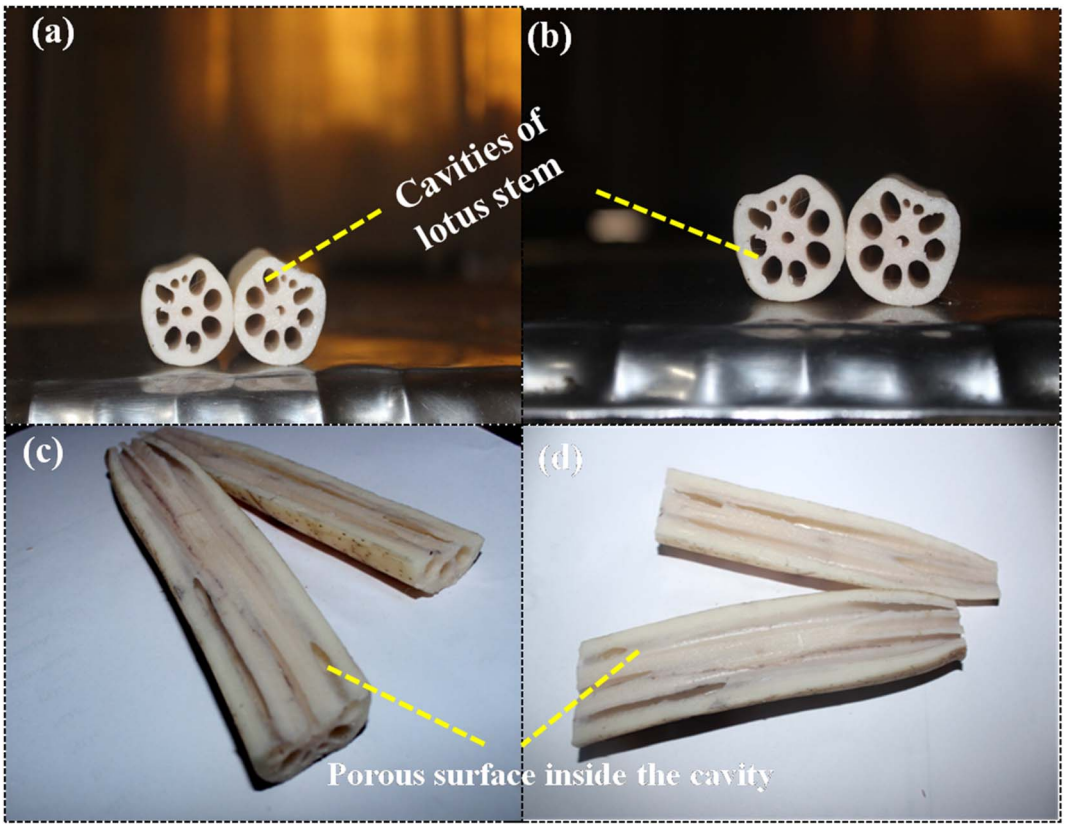

Fig. 3 Lateral and horizontal cross-sections of the lotus stem describing the porous cavity throughout the length of the stem.

for synthesizing a biochar-zerovalent composite, keeping in view the porous nature that could incorporate the metal as well as providing a high surface area for analyte interaction. However, it is possible only if the porous nature and cavity-type structure of the lotus stem are maintained even after the event of initial treatment through annealing. To get an insight into that, we carried out the FE-SEM analysis of the material after annealing and incorporation of metal.

The surface morphology of nZVI and the nZVI@Biochar nanocomposite was examined by scanning electron microscopy. From the FE-SEM micrographs, we can see the monodisperse spherical particles of nZVI with particle sizes in the 100 nm range (see Fig. 4a and b). The FE-SEM micrographs of porous bare biochar show cavity-like structures within the biochar matrix (see Fig. 4c and d). We observed that the biochar retained the cavity and tubular-like structures of its parent lotus stem biomass material, during pyrolysis.

Furthermore, the tubular cavities in the biochar are expected to offer an ideal environment for decorating nZVI nanoparticles and the adsorption and interaction of contaminants such as glyphosate (see Fig. 5a and b). The impregnation of nZVI nanoparticles within the biochar cavity prevents the agglomeration of these nZVI particles (Fig. S1, ESI†). Moreover, TEM micrographs manifested the successful loading of nZVI onto the biochar surface with less agglomeration of nZVI particles (see Fig. 5c and d). To determine the composition of the as-synthesized material, we have carried out elemental analysis as shown in Fig. S2, ESI.† As can be seen from the elemental mapping, the final synthesized material possesses 30.3 wt% iron with nearly uniform distribution over the composite.

3.2. Electrochemical studies

To analyze the application of the as-synthesized materials for electrochemical sensing, we have drop casting the as-prepared material (nZVI@Biochar) dispersed in isopropyl alcohol (IPA) on a glassy carbon electrode, and carried out cyclic voltammetric analysis for glyphosate sensing. The nZVI@Biochar-modified electrodes demonstrated a reduction peak around −0.3 V, corresponding to glyphosate. To confirm it further, we carried out a similar analysis with parent materials, biochar, and nZVI; we didn't find out any such response in the cyclic voltammetric study (see Fig. 6a). Also, it is quite evident from Fig. 6a that in the absence of nZVI no reaction occurs. The presence of other metal ions in parent biochar should react even in the absence of nZVI which should have got reflected in the cyclic voltammogram (Fig. 6a, red trace). However, a clear peak is visible only with iron-containing biochar (Fig. 6a, green trace). These results clearly suggest that iron acts as the electrocatalyst for the sensing of glyphosate.

Besides, the effect of pH ranging from 2–9 on the behavior of the nZVI@Biochar electrode was examined (see Fig. 6b). There

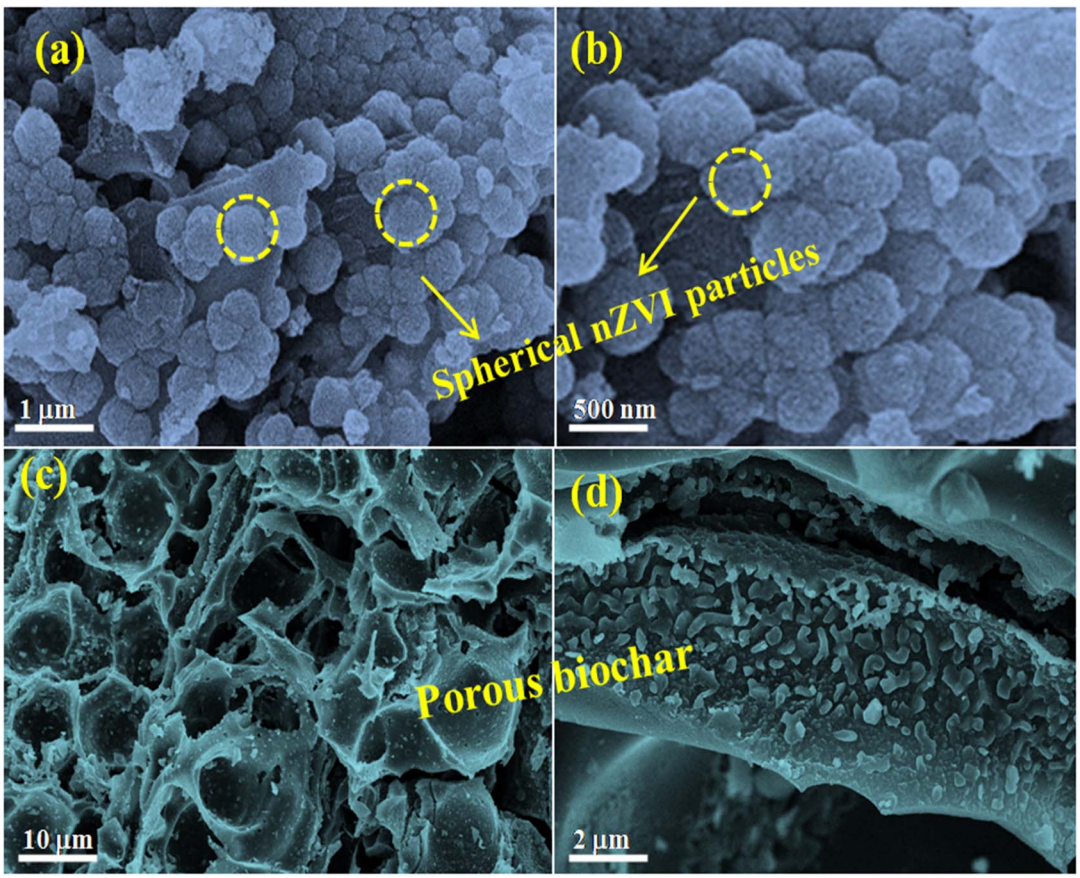

Fig. 4 FE-SEM micrograph analysis of (a and b) the as-synthesized nZVI particles and (c and d) porous surface of biochar.

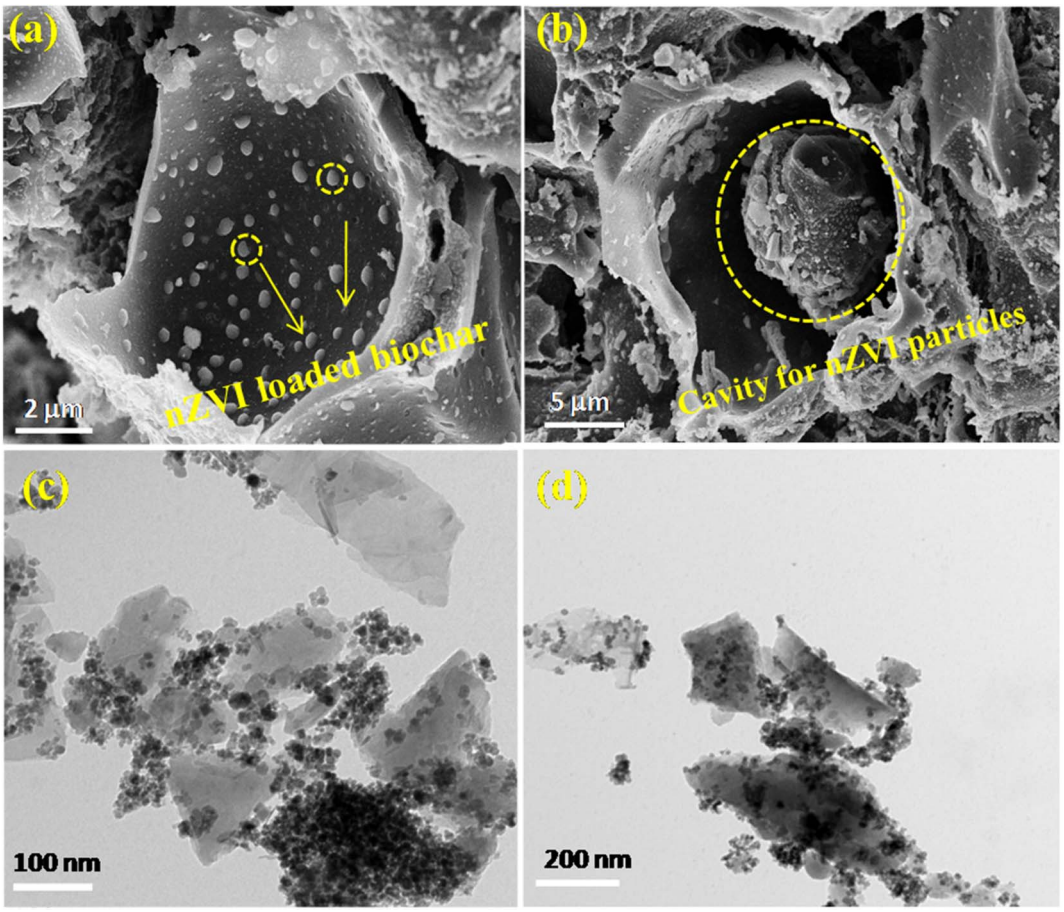

Fig. 5 FE-SEM micrograph analysis of (a and b) the nZVI@Biochar composite confirming loading of nZVI on the biochar surface, and (c and d) TEM micrographs of the nZVI@Biochar composite.

was no significant shift in the reduction peak of glyphosate with an increase in the pH. However, the maximum current intensity was observed at pH = 7. This may be due to the deprotonation of glyphosate functional groups that resulted in its increase in complexation potential with the iron metal cluster which consequently enhances the sensing response of the nZVI@-Biochar electrode.

After the initial analysis with cyclic voltammetry (see Fig. S3, ESI†), we carried out linear sweep voltammetry (LSV) with varying concentrations of glyphosate in the electrolyte on the nZVI@Biochar modified electrode. As can be seen from Fig. 7, the peak current increases with an increase in the concentration of glyphosate in the electrolyte, confirming that the reduction peak is due to glyphosate. The peak current shows a linear

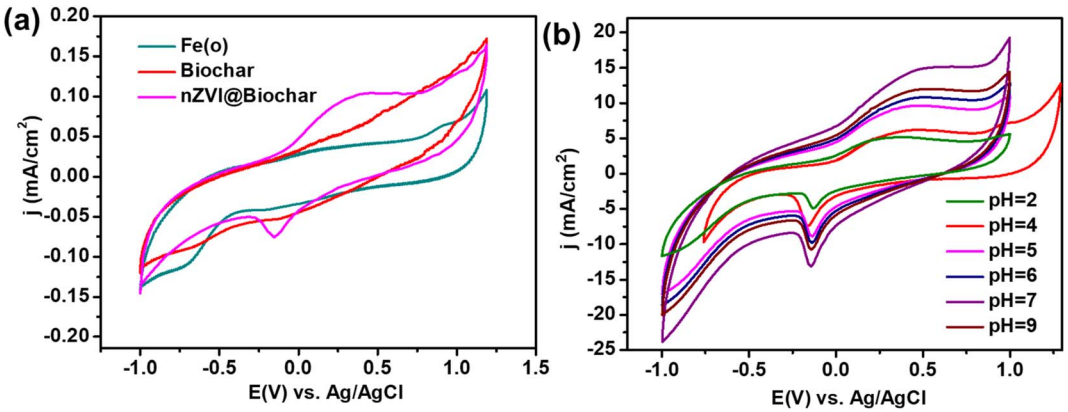

Fig. 6 Cyclic voltammograms of (a) nZVI@Biochar, biochar, and nZVI in 0.1 M KNO_3 with 10 ppm glyphosate concentration and (b) effect of pH ranging from (2–9) on the performance of the nZVI@Bicohar electrode.

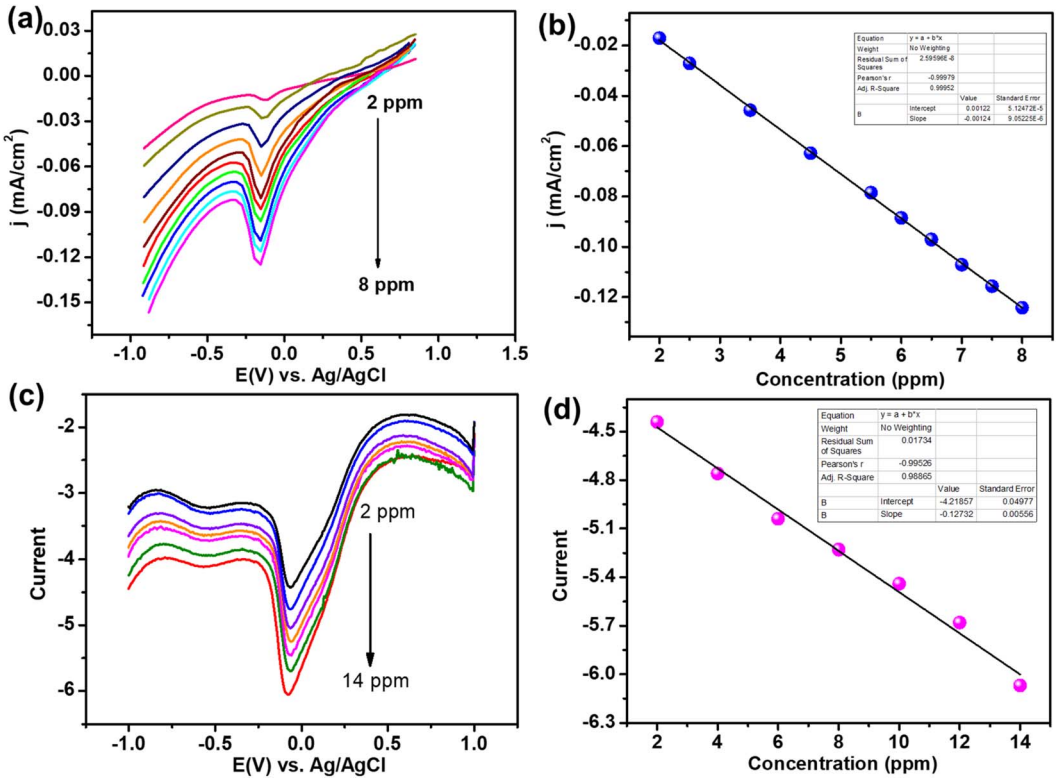

Fig. 7 (a) linear sweep voltammograms at different concentrations of glyphosate on the nZVI@Biochar electrode and (b) corresponding peak current *versus* concentration plot, (c) differential pulse voltammograms with varying glyphosate concentration on the nZVI@Biochar electrode, and (d) corresponding current *vs.* concentration plot.

relationship with a concentration range from 2–8 ppm. This linear response prompted us to analyze this material further for glyphosate sensing. To carry out the sensing efficiency of nZVI@Biochar for glyphosate, we carried out differential pulse voltammetry (DPV) at different concentrations of glyphosate in the electrolyte. As expected, the peak current increases with increasing concentration of glyphosate and an increase in current demonstrated a linear response, which is a prerequisite for any sensor. The critical parameters for any sensing materials are sensing efficiency denoted by the limit of detection and its stability. We have calculated the LOD from the current *vs.* concentration response in DPV analysis which was determined to be 0.13 ppm. Both LSV and DPV analyses demonstrate the efficient sensing capability of nZVI@Biochar towards glyphosate.

3.3. Stability and reusability studies

To check the stability, we have carried out a long-term constant current test, *i.e.*, chronopotentiometry analysis, which

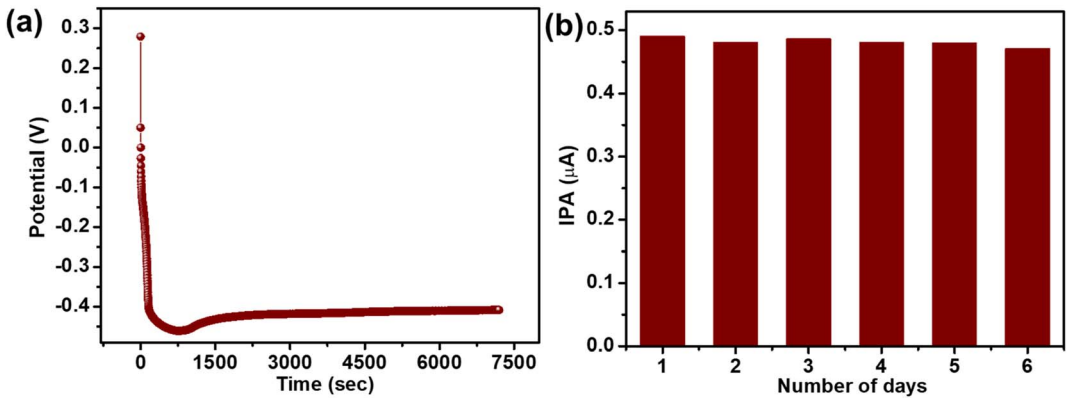

Fig. 8 (a) Chronopotentiometric plot of the nZVI@Biochar electrode for 2 hours at a 10 mA cm^{-2} scan rate. (b) The current response shows the stability of the nZVI@Biochar electrode for 7 days with an inset bar graph depicting the slight change in current after being reused again and again.

Table 1 Limit of detection of various modified electrode sensors for the detection of glyphosate

S. no.	Sensors	Method	Limit of detection (LOD)	References
1	CuAl-LDH/Gr nanocomposite	Stripping voltammetry	1×10^{-9} M	13
2	Graphite powder/mineral oil paste electrode	Square wave voltammetry	2×10^{-9} M	32
3	Cu-BTC MOF	Differential pulse voltammetry	1.4×10^{-13} M	11
4	Carbon paste electrode-modified biochar copper(II) hexadecafluoro-29*H*,31 phthalocyanine complex	Square wave voltammetry	2×10^{-8} M	33
5	Organophilic silane in the interlayer space of acid-treated smectite	Square wave voltammetry	9.8×10^{-7} M	34
6	Horseradish peroxidase polymeric matrix	Cyclic voltammetry	1.7×10^{-6} M	35
7	Copper nanoparticles and reduced graphene oxide	Differential pulse voltammetry	1.9×10^{-7} M	36
8	Cu-BTC MOF/g-C_3N_4	Photocurrent	1.3×10^{-13}M	37
9	Graphite oxide sensor	Square wave voltammetry	1.7×10^{-8}M	38
10	nZVI@Biochar	Differential pulse voltammetry	7×10^{-7} M (0.13 ppm)	This work

demonstrated a stable current for more than 2 hours (see Fig. 8a). The chronopotentiometry stability curve after the initial voltage drop, also known as polarization loss from 0.4 V to −0.3 V, maintains a flat trace demonstrating a very stable electron transfer process between the electrode and electrolyte, which is essential for the electrochemical sensor. Moreover, to access the stability of the modified (nZVI@Biochar) electrode, the electrodes were kept covered in a dry environment for 7 days and the voltammetric response was analyzed for 7 consecutive days (see Fig. 8b). It was observed that there was no sharp drop in the current intensity of the nZVI@Biochar electrode, which suggested that the electrode can be reused again and again.

In addition to this, the limit of detection of the nZVI@-Biochar sensor towards glyphosate was compared with other sensors already reported in the literature as shown in Table 1.

3.4. Computational studies

To get an insight into electrochemical studies, DFT studies were carried out by using the Lee–Yang–Parr correlation functional (B3LYP) and LanL2DZ basis set for the Fe atom and 6–311 g (d,p) for non-metal atoms. For biochar, we have selected coronene ($C_{24}H_{12}$) as a model material,[39,40] and the optimized geometries of glyphosate-biochar, nZVI@Biochar, and the nZVI@Biochar–glyphosate composite system are shown in Fig. 9(a–c). The cartesian coordinates of these optimized geometries are shown in the table (T1, ESI†).

After optimizing the geometries of each of the materials, we calculated the interaction energies of glyphosate with biochar and the composite. As for the electrochemical transformations, favorable interaction between glyphosate and the material is a prerequisite. The interaction energies of glyphosate with both biochar and composite materials were calculated based upon optimized geometries. The interaction energy of the energetically favorable configuration of glyphosate-biochar ($E_{\text{gly-BC}}$), nZVI@Biochar ($E_{\text{BC-nZVI}}$), and nZVI@Biochar-glyphosate ($E_{\text{gly-BC-nZVI}}$) was calculated by using the following equation shown:

$$\Delta E = E_{\text{complex}} - [E_{\text{gly-BC}} + E_{\text{gly-BC-nZVI}}] \quad (2)$$

Moreover, to validate our results and for higher accuracy, we have calculated basis set superposition error (BSSE)[41] by employing eqn (3)

$$\Delta E_{\text{int}}\left(E_{\text{gly-BC-nZVI}}\right) = E\frac{\text{gly-BC-nZVI}}{\text{gly-BC-nZVI}}(\text{gly-BC-nZVI}) - E\frac{\text{BC-nZVI}}{\text{BC-nZVI}}(E_{\text{BC-nZVI}}) - E\frac{\text{gly-BC}}{\text{gly-BC}}(\text{gly-BC}) \quad (3)$$

where $E\frac{\text{gly-BC-nZVI}}{\text{gly-BC-nZVI}}(\text{gly-BC-nZVI}) - E\frac{\text{BC-nZVI}}{\text{BC-nZVI}}(E_{\text{BC-nZVI}}) - E\frac{\text{gly-BC}}{\text{gly-BC}}(\text{gly-BC})$ represents the energies of nZVI@Biochar-glyphosate, nZVI@Biochar, and glyphosate-biochar respectively.

The calculated interaction energy value of glyphosate biochar was found to be −598.614 kJ mol^{-1} and its counterpoise interaction energy values were found to be −631.9965 kJ mol^{-1}. Similarly, the interaction energy value for nZVI@Biochar-glyphosate was found to be −1417.77 kJ mol^{-1} and its corrected counterpoise interaction energy was determined to be −1575.3 kJ mol^{-1}. Therefore, the basis set superposition error was found to be −33.3825 kJ mol^{-1} and −157.53 kJ mol^{-1} for glyphosate-biochar and nZVI@Biochar-glyphosate, respectively. This error is found to be very small, which is indicative of the accuracy of our calculated results.

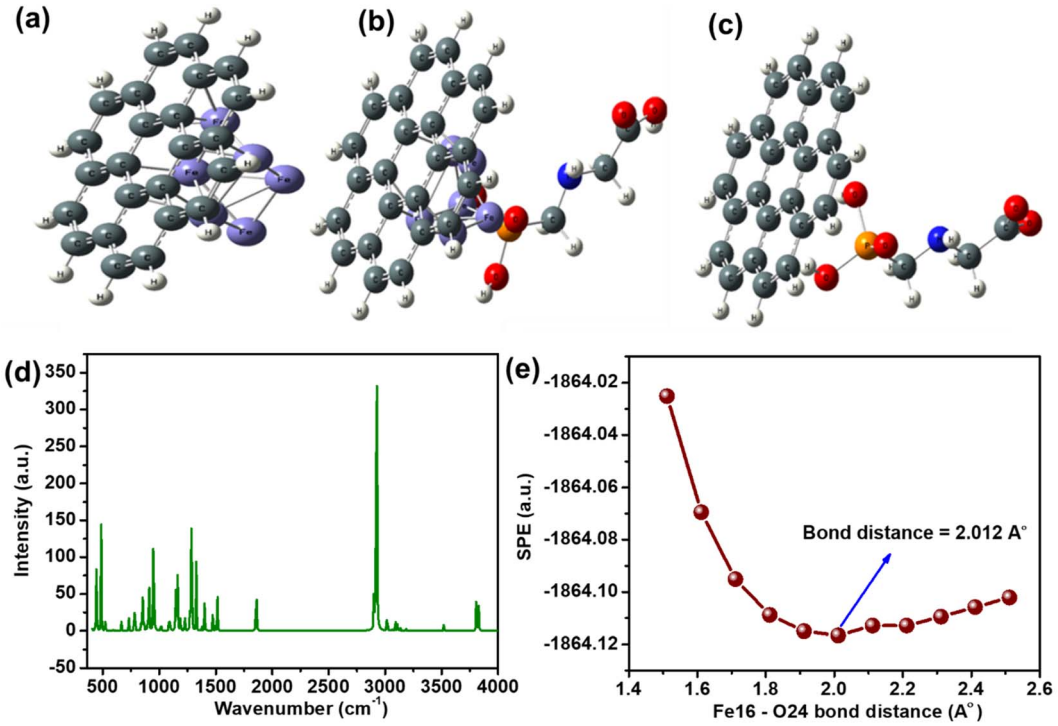

Fig. 9 DFT optimized geometries of (a) nZVI@Biochar, (b) biochar-glyphosate and (c) nZVI@Biochar-glyphosate. The color red indicates oxygen; white indicates hydrogen; grey indicates carbon; blue indicates nitrogen; orange indicates phosphorous. DFT calculated (d) IR spectrum and (e) single point energy plot for nZVI@Biochar with glyphosate.

In addition to this, the interaction energy of glyphosate-biochar got enhanced with the incorporation of nZVI in the complex, predicting better chemical interaction between the biochar-glyphosate functional moieties with Fe(0). To confirm these interactions, we have carried out theoretical IR (Fig. 9d), which is in line with IR carried out experimentally. In addition to this, the preferential site of interactions in the composite material was found to be the feat (positon-16) of nZVI and oxygen at position 24 (O-24) of glyphosate. Single point energy (SPE) scans were carried out to find the bond distance between Fe-16 nZVI and O-24 at which the interaction is maximum (Fig. 9e). All of these suggest a favorable interaction between Fe and glyphosate, which is not the case with the biochar.

Apart from interaction, the critical factor that decides electron transfer between the electrode and analyte is the HOMO–LUMO energy gap of biochar-glyphosate and nZVI@Biochar-glyphosate systems. The lower the HOMO–LUMO gap the smaller the energy barrier for electron transfer (the activation overpotential) between the electrode and analyte in the electrolyte. To get an insight into this, we explored the frontier molecular orbitals (FMOs) and performed molecular electrostatic potential (MEP) calculations upon the interaction of biochar and nZVI@Biochar with the glyphosate system (see Fig. 10a). The calculated band gap energy values and other possible HUMO–LUMO orientations shown in (T2, and Fig. S4, ESI†) demonstrate that the band gap decreases noticeably by the incorporation of zero-valent Fe into the biochar-glyphosate system. Furthermore, we also calculated the band gap energy values of Fe(0), Fe_2O_3, and Fe_3O_4 with glyphosate (Fig. S5, ESI†). The band gap energy value was found to be more in the case of the Fe_2O_3-glyphosate and Fe_3O_4-glyphosate systems in comparison to Fe(0)-glyphosate, which is not suitable for feasible electron transfer. From these observations, we can also conclude that Fe(0) plays a major role in the electrochemical catalysis of glyphosate.

To verify the results, we calculated the density of states (DOS) in the biochar-glyphosate composite with and without nZVI. In the case of biochar-glyphosate, the density of states is low, but the incorporation of nZVI in the composite results in a sudden jump in the DOS (see spectra in Fig. 10b). It is known that an increase in the DOS results in a decrease in the band gap, which is a direct representation of a reduction in the energy gap. All these results suggest facile electron transport between glyphosate and the nZVI@Biochar composite, which could be exploited for designing an efficient sensing platform for glyphosate in aqueous media. This positive interaction between the nZVI@Biochar composite and glyphosate is also supported by a low HOMO–LUMO gap and high DOS, thus strengthening the results obtained through CV and DPV (Fig. 6 and 7).

The same is further supported by MEP, which allows us to visualize the variable charge distribution within the molecule. The red regions indicate electron-rich regions, whereas the green regions indicate neutral areas. As is evident from Fig. 10c with the incorporation of nZVI in GLY-BC (Glyphosate-Biochar), the red region around the biochar increases compared to the parent biochar materials on account of the presence of iron in

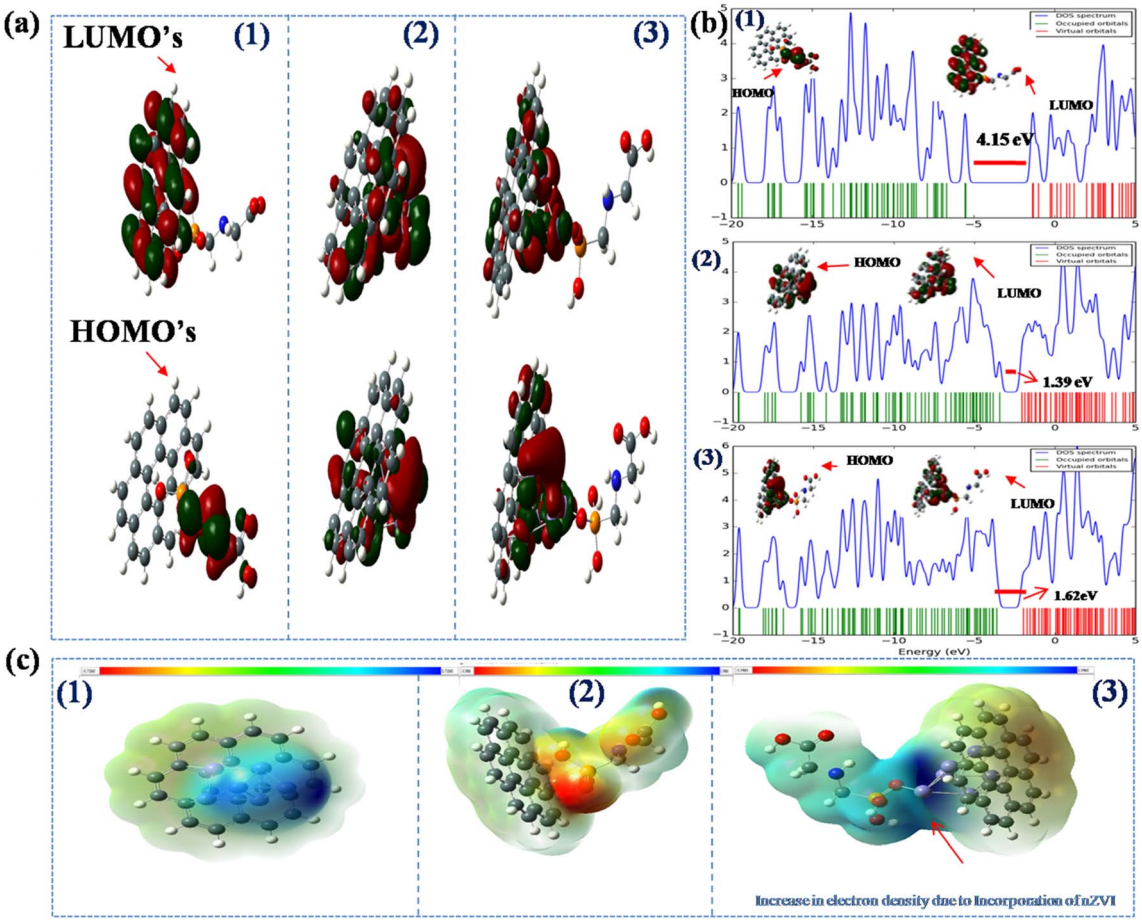

Fig. 10 (a) DFT calculated HOMO and LUMO of (1) nZVI@Biochar, (2) upon the interaction of biochar with glyphosate and (3) nZVI@Biochar with glyphosate. (b) The DOS spectra of (1) nZVI@Biochar and (2) biochar with glyphosate and nZVI@Biochar with glyphosate. (c) Molecular electrostatic potential images of (1) nZVI@Biochar, (2) the interaction of biochar with glyphosate and (3) nZVI@Biochar with glyphosate.

the biochar indicating a negative electrostatic potential. The increase in the electron density due to the incorporation of nZVI results in higher reducing power of the composite towards the glyphosate, which is in line with the electrochemical data.

Taken together, both experimental and theoretical calculations suggest better electrochemical reduction dynamics compared to the biochar alone. In the case of nZVI@Biochar, the Fe center acts as a mediator as no reduction peak was observed with biochar alone (see Fig. 6a). Since it is an inner sphere electron transfer reaction, the analyte is required to have a favorable interaction with the electrocatalyst. As mentioned above, the interaction energy of glyphosate-biochar got enhanced with the incorporation of nZVI in the complex, predicting better chemical interaction between the biochar-glyphosate functional moieties and Fe(0).

With this, we came to a conclusion why nZVI@Biochar is better suited compared to biochar alone. Secondly, the inner sphere electrochemical transformations occur *via* interaction between the analyte and catalytic site on the electrocatalyst. The preferential site of interactions in the composite material was found to be Fe at (positon-16) of nZVI and oxygen at position 24 (O-24) of glyphosate as discussed above. This is in line with our experimental results that suggest a facile electrochemical charge transfer incorporation of nZVI on biochar. Thus, nZVI acts as both an interaction site and an electrocatalytic reaction/sensing site.

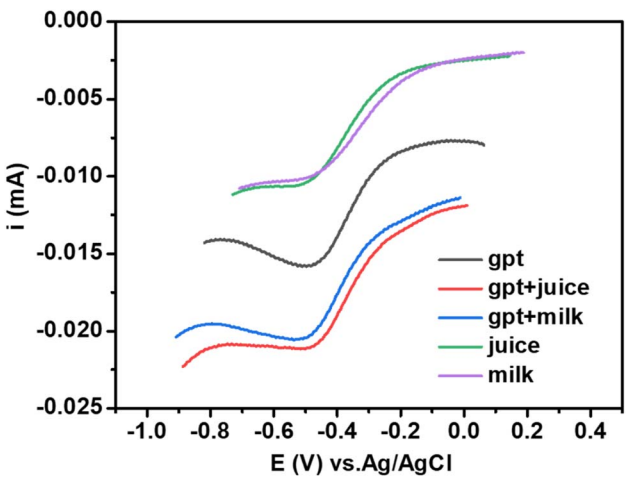

Fig. 11 Linear sweep voltammograms of spiked samples of milk and juice with a known amount of glyphosate.

Table 2 Sensing of glyphosate in environmental samples by using the nZVI@Biochar sensor

	Glyphosate (real)	Before spiking (unspiked)	After spiking (spiked)	Recovery factor
Milk	0.0105 mA	0.0102 mA	0.0204 mA	97%
Juice	0.0105 mA	0.0106 mA	0.0212 mA	101%

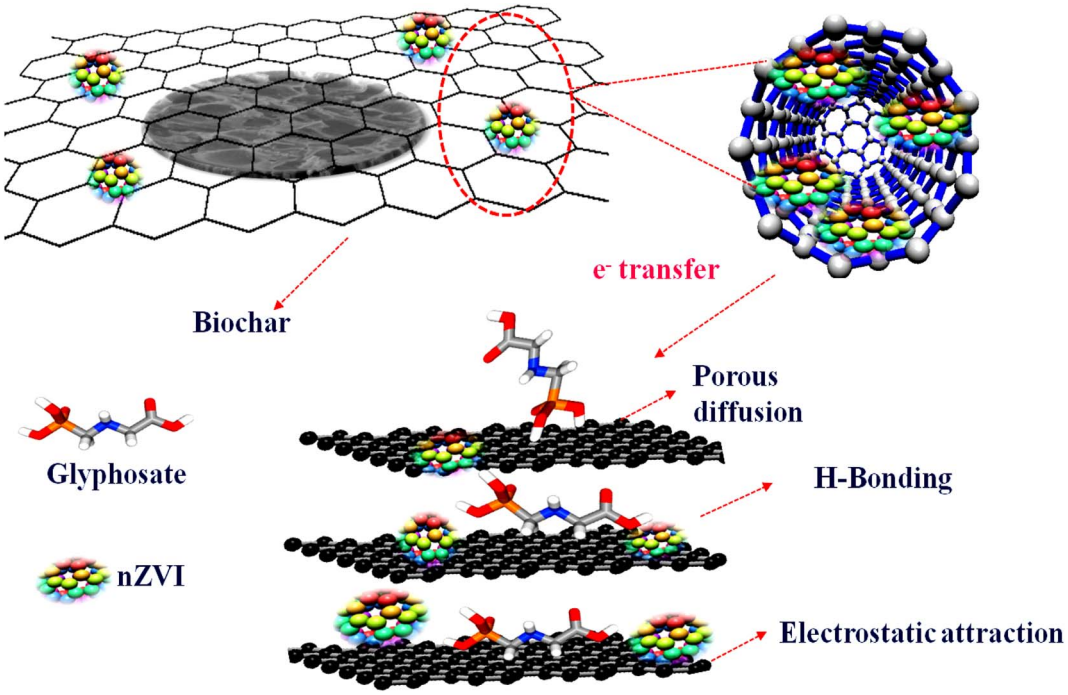

Scheme 2 Probable mechanism for sensing of glyphosate by nZVI@Biochar.

3.5. Real sample analysis

To analyze the practical applicability of the sensor for real sample analysis, we calculated the recovery factor.[42,43] This was estimated through linear sweep voltammetry by spiking juice and milk samples with known amounts of glyphosate (see Fig. 11). The as-synthesized composite demonstrated excellent results in glyphosate detection with an excellent recovery rate in the range of 101–90% (Table 2), and the relative standard deviation was less than 3%. Moreover, to check the selectivity of the composite material towards glyphosate sensing, we carried out cyclic voltammetry with similar molecules, Fig. S6, ESI.† As can be seen from cyclic voltammograms (Fig. S6, ESI†), the response of these molecules falls in different potential regions with the least chances of interference with a glyphosate electrochemical reaction. Both the interference studies and spiking and recovery method suggest the feasibility of the present sensing platform for electrochemical sensing of glyphosate.

3.6. Mechanism of sensing of glyphosate by nZVI@Biochar

Based on the experimental and DFT calculations, a plausible mechanism for glyphosate sensing requires the presence of both biochar and nZVI in the electrode. As the charge transfer is highly enhanced due to the incorporation of nZVI in the composite, it points towards the fact that the metal atom acts as a site of electron transfer between the electrode and glyphosate. The presence of biochar with a cavity-like structure and negatively charged surface functional groups (like OH as suggested by IR) attracts the glyphosate and provides a surface site by holding the analyte through hydrogen bonding and electrostatic interactions (Scheme 2). Thus the high surface area in combination with the electrostatic and hydrogen bonding interactions of the biochar complements the excellent charge transfer properties of the catalytic Fe metal center. Furthermore, it can be deduced that the synergetic effect of biochar and zerovalent iron is essential for the effective sensing of glyphosate. In general, the probable mechanisms for the sensing of glyphosate with the Fe-based biochar seems to be primarily porous diffusion, electrostatic and H-bonding interactions, and importantly complexation by the iron metal center.

4. Conclusions

To summarise, we report a composite material based upon biochar and a zero-valent metal, which exhibited efficient sensing properties towards glyphosate in an aqueous medium.

The parent material biochar was obtained from a naturally occurring lotus stem by carbonizing in a muffle furnace. The nZVI@Biochar composite, through analysis with various physicochemical techniques, suggested a cavity and tubular-like structure with oxygen-rich functionalities. The presence of zerovalent metal ions in the cavity of biochar resulted in highly favorable interaction with glyphosate, as suggested by the interaction energies from DFT calculations. The as-synthesized composite exhibited high activity toward electrochemical sensing of glyphosate in the aqueous medium. LSV as well as DPV analysis suggested a linear increase in current with concentration, which leads to increased sensitivity and a LOD of 0.13 ppm, which are well within the WHO guidelines. The composite exhibited not only quite a high efficiency but also very high stability as suggested by chronopotentiometry. Moreover, the prepared sensor also exhibits excellent recovery close to or above 1 for biological samples. We believe that this report brings light to the design of new materials based on naturally occurring raw materials with simple synthetic pathways and zero-valent metal ions, which are usually un-utilized for electrochemical transformations.

Author contributions

Aaliya Qureashi: data curation, experimentation, investigation, methodology, and original draft. Altaf Hussain Pandith: conceptualization, project administration, supervision, resources, review, and editing. Arshid Bashir: investigation, methodology, review, and editing. Lateef Ahmad Malik: experimentation, writing, review, and editing. Taniya Manzoor: DFT calculations and writing. Faheem A Sheikh: writing, review, and editing. Kaniz Fatima: DFT studies. Zia-ul-Haq: review and editing.

Conflicts of interest

The authors declare no conflicts of interest.

Acknowledgements

We acknowledge the Department of Science & Technology, Government of India, New Delhi, for providing facilities under the DST-PURSE Programme (TPN-56945) to the Department of Chemistry, University of Kashmir. We are also thankful to NIT Srinagar for providing FE-SEM and STIC Coaichin for providing TEM faculty for this work.

References

1 R. Liu, Y. Xie, K. C. J. Xie, Y. Zhang and Y. Huang, *J. Phys. Chem. Solids*, 2022, **161**, 110403.
2 R. T. A. Carneiro, T. B. Taketa, R. J. G. Neto, J. L. Oliveira, E. V. R. Campos, M. A. de Moraes, C. M. G. da Silva, M. M. Beppu and L. F. Fraceto, *J. Environ. Manage.*, 2015, **151**, 353–360.
3 C. Zhang, Y. She, T. Li, F. Zhao, M. Jin, Y. Guo, L. Zheng, S. Wang, F. Jin, H. Shao and H. L. J. Wang, *Anal. Bioanal. Chem.*, 2017, **409**, 7133–7144.
4 D. Guo, N. Muhammad, C. Lou, D. Shou and Y. Zhu, *New J. Chem.*, 2019, **43**, 121–129.
5 C. Hidalgo, C. Rios, M. Hidalgo, V. Salvadó, J. V. Sancho and F. Hernández, *J. Chromatogr. A*, 2004, **1035**, 153–157.
6 S. Y. Chang and M. Y. Wei, *J. Chin. Chem. Soc.*, 2005, **52**, 785–792.
7 A. Royer, S. Beguin, J. C. Tabet, S. Hulot, M. A. Reding and P. Y. Communal, *Anal. Chem.*, 2000, **16**, 3826–3832.
8 M. Motojyuku, T. Saito, K. Akieda, H. Otsuka, I. Yamamoto and S. Inokuchi, *J. Chromatogr. B: Anal. Technol. Biomed. Life Sci.*, 2008, **875**, 509–514.
9 S. Shrivastava, A. Kumar, N. Verma, B. Y. Chen and C. T. Chang, *Electroanalysis*, 2020, **32**, 1–10.
10 F. C. Moraes, L. H. Mascaro, S. A. S. Machado and C. M. A. Brett, *Electroanalysis*, 2010, **22**, 1586–1591.
11 Y. Cao, L. Wang, C. Shena, C. Wang, X. Hua and G. Wan, *Sens. Actuators, B*, 2019, **283**, 487–494.
12 F. Zouaouia, S. Bo. Bacha, M. Bourouina, I. A. Nemeira, H. B. Halima, J. G. Gonzaleza, N. E. A. E. Hassania, A. Alcacer, J. Bausells, N. J. Renault, N. Zine and A. Errachid, *Sens. Actuators, B*, 2020, **309**, 127753.
13 C. Zhang, X. Liang, Y. Lu, H. Li and X. Xu, *Sensors*, 2020, **20**, 4146.
14 C. Zhang, Y. She, T. Li, F. Z. M. Jin, Y. G. L. Zheng, S. Wang, F. J. H. Shao, H. Liu and J. Wang, *Anal. Bioanal. Chem.*, 2017, **409**, 7133–7144.
15 S. Zavareh, Z. Farrokhzad and F. Darvishi, *Ecotoxicol. Environ. Saf.*, 2018, **155**, 1–8.
16 S. L. C. Muñoz, M. A. G. Fuentes, L. A. O. Frade, E. Torres, S. Talu, G. Trejo and A. M. Albores, *Electroanalysis*, 2019, **31**, 927.
17 P. C. Oliveira, E. M. Maximiano, P. A. Oliveira, J. S. Camargo, A. R. Fiorucci and G. J. Arruda, *J. Environ. Sci. Health, Part B*, 2018, **53**, 817.
18 A. Bashir, A. H. Pandith, A. Qureashi, L. A. Malik, M. Gani and J. M. Perez, *J. Environ. Chem. Eng.*, 2022, **17**, 107401.
19 M. Zhang, B. Gao, S. Varnoosfaderani, A. H. Y. Yao and M. Inyang, *Bioresour. Technol.*, 2013, **130**, 457–462.
20 L. Z. Gang, Z. F. Shen and R. Sasai, *Chem. Eng. J.*, 2010, **160**, 57–62.
21 R. Li, H. Deng, X. Zhang, J. J. Wang, M. K. Awasthi, Q. Wang, R. Xiao, B. Zhou, J. Du and Z. Zhang, *Bioresour. Technol.*, 2019, **273**, 335–340.
22 Y. T. Wei, S. C. Wu, C. M. Chou, C. H. Che, S. M. Tsai and H. L. Lien, *Water Res.*, 2010, **44**, 131–140.
23 T. Pasinszki and M. Krebsz, *Nanomaterials*, 2020, **10**, 917.
24 Y. T. Lin, C. H. Weng and F. Y. Chen, *Sep. Purif. Technol.*, 2008, **64**, 26–30.
25 M. L. Tran, S. W. Deng, C. C. Fu and R. S. Juang, *Environ. Sci. Pollut. Res.*, 2020, **27**, 30853–30867.
26 M. M. Tarekegn, A. M. Hiruy and A. H. Dekebo, *RSC Adv.*, 2021, **11**, 18539–18551.
27 Q. Li, Z. Chen, H. Wang, H. Yang, T. Wen, S. Wang, B. Hu and X. Wang, *Sci. Total Environ.*, 2021, **792**, 148546.

28 G. Wei, J. Zhang, J. Luo, H. Xue, D. Huang, Z. Cheng and X. Jiang, *Front. Environ. Sci. Eng.*, 2019, **13**, 61.
29 A. Qureashi, A. H. Pandith, A. Bashir and L. A. Malik, *Anal. Methods*, 2021, **13**, 4756–4766.
30 A. S. Eltaweil, H. A. Mohamed, E. M. A. El-Monaem and G. M. El-Subruiti, *Adv. Powder Technol.*, 2020, **31**, 1253–1263.
31 X. Jiang, Z. Ouyang, Z. Zhang, C. Yang, X. Li, Z. Danga and P. Wu, *Colloids Surf., A*, 2018, **547**, 64–72.
32 P. C. Oliveira, E. M. Maximiano, P. A. Oliveira, J. S. Camargo, A. R. Fiorucci and G. J. Arruda, *J. Environ. Sci. Health, Part B*, 2018, **53**, 817–823.
33 A. Wong, D. G. de Lima, P. A. Ferreira, S. Khan, R. A. B. da Silva, J. L. B. de Faria, M. D. Pilar and T. Sotomayor, *J. Appl. Electrochem.*, 2021, **51**, 761–768.
34 J. G. Y. Mbokana, G. K. Dedzo and E. Ngameni, *Appl. Clay Sci.*, 2020, **188**, 1055113.
35 E. A. Songa, O. AArotiba, H. O. O. Joseph, N. Jahed, P. G. L. Baker and E. I. Iwuoha, *Bioelectrochemistry*, 2009, **75**, 117–123.
36 S. Setznagl and I. Cesarin, *Int. J. Environ. Anal. Chem.*, 2022, **102**, 293–305.
37 Y. Cao, L. Wang, C. Wang, X. Hu, Y. Liu and G. Wang, *Electrochim. Acta*, 2019, **317**, 341–347.
38 J. S. Santos, M. S. Pontes, E. F. Santiago, A. R. Fiorucci and G. J. Arruda, *Sci. Total Environ.*, 2022, **749**, 142385.
39 N. K. A. Shafiekhani, *Phys. E*, 2013, **47**, 309–315.
40 J. Ma, A. Michaelides and D. Alfè, *J. Chem. Phys.*, 2011, **134**, 134701.
41 S. D. Sherilli, *Counterpoise Correction and Basis Set Superposition Error*, School of chemistry and Bichemistry, 2010.
42 H. Ping, F. Zhao, C. Li, B. Wang, H. Kong, Y. Li and Z. Ma, *Sepu*, 2022, **40**, 273–280.
43 S. V. Kergaravat, S. N. Fabiano, A. R. Soutullo and S. R. Hernandez, *Microchem. J.*, 2021, **160**, 105654.